

Interactive Residual Stress Modeling for Soft Tissue Simulation

Jun Wu[†], Kai Bürger[‡], Rüdiger Westermann[§] and Christian Dick[¶]

Computer Graphics & Visualization Group, Technische Universität München, Germany

Abstract

Residual stress is the stress which remains in a deformable body in the absence of external forces. Due to the release of residual stress after cutting, soft tissues will shrink and the wound will open. Thus, to realistically simulate soft tissue deformations due to cutting, a model for the residual stress in a patient body is needed. In this paper we present an interactive method to compute a physically meaningful patient-specific residual stress distribution. With our method, by using their experience doctors can sketch directional stress strokes and specify stress magnitudes at a few control points on the body surface. The residual stress is then immediately computed from these inputs and visualized by displaying the deformations of a set of control cuts on the body. In a visually guided session, the user can further modify the initial strokes and magnitudes until a satisfactory result is obtained. We demonstrate the potential of the proposed method for virtual cut simulation by showing the variations of wound openings depending on the residual stress distribution.

Categories and Subject Descriptors (according to ACM CCS): I.3.5 [Computer Graphics]: Computational Geometry and Object Modeling—Physics-based modeling I.6.7 [Simulation and Modeling]: Simulation Support Systems—J.3 [Life and Medical Science]: Medical information systems—

1. Introduction

The input models used in computer-aided surgery simulation are typically generated from patient-specific scans such as CT or MRI. In these scans, the internal stress distribution of the measured tissue is lost. However, even in the absence of external forces soft tissue is not stress free, but it is tensioned by the so-called *residual stress*. The residual stress is a non-negligible factor in soft tissue dynamics [Hum03], and its effect is especially apparent when soft tissue is cut. After cutting, the tissue will shrink and the wound will open due to the release of residual stress [CF86]. Moreover, the shrinkage of a flap due to the relaxation of residual stress affects the quality of surgeries, e.g., a breast reconstruction surgery, in which the volume of the flap is of crucial importance [KZPB04]. Therefore, to produce physically realistic

cutting simulations for soft tissue, patient-specific models of the residual stress need to be derived and included in the simulation.

However, despite the importance of residual stress for soft tissue dynamics, it is not well addressed in biomedical simulation. This is due to the fact that the residual stress distribution is patient-specific, but no procedure yet exists to derive this distribution directly from non-invasive tissue measurements. The residual stress is valued by a second order tensor which can be decomposed into principal directions (eigenvectors) and principal stresses (eigenvalues). The values of principal stresses vary strongly between different individuals, e.g., tight or loose. Moreover, the principal directions are geometry dependent and vary spatially. Even though models for these distributions in the human body exist, these models cannot easily be parameterized to a particular body.

In this paper, we present an interactive method to derive a physically meaningful residual stress distribution for a given patient model, and we use this distribution for estimating the opening of cuts in soft tissue (see Figure 1 and the attached video). The stress model is interactively designed by

[†] wujun.buaa@gmail.com

[‡] buerger@tum.de

[§] westermann@tum.de

[¶] dick@tum.de

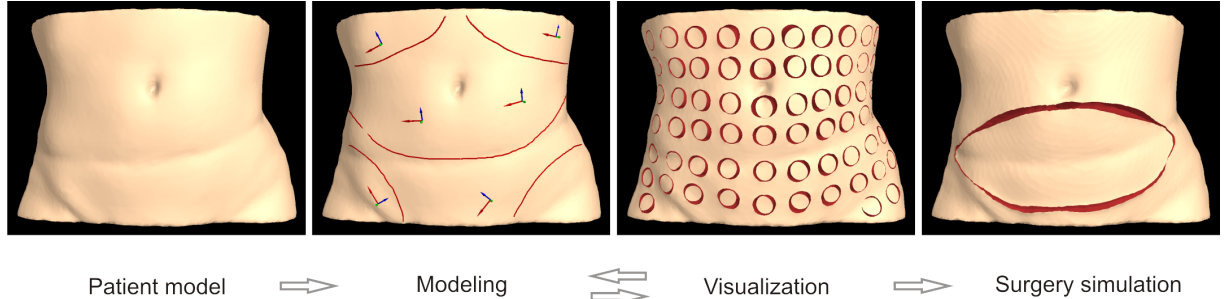


Figure 1: Overview of the modeling procedure. First, a patient specific volumetric CT scan is used as input model. Next, an experienced surgeon designs a residual stress tensor field by drawing stress directions via strokes on the model surface, and by specifying the stress magnitudes at several sparse locations. A global tensor field is constructed from this information via Laplacian interpolation, while the equilibrium equations serve as a penalty term. The tensor field is immediately visualized by simulating the effects of making many small holes on the surface. Based on the feedback, the surgeon can modify her design until a satisfied tensor field is computed. Finally, this residual stress is used in a biomedical simulation of the opening of wounds due to cuts.

a domain expert based on her expertise about the residual stress distribution in human bodies of different shape and consistency. The design process is subject to additional constraints, which enforces that the resulting model respects certain physical laws. The modeling result is visualized immediately, and thus allows interactive control over the residual stress distribution.

The specific contributions of our paper are:

- *A procedure to interactively model the residual stress distribution in patient specific models.* Following the well-known concept of Langer's lines [Lan78] in anatomy, the user draws several strokes on the surface of soft tissues, thus specifying a coarse skeleton of the distribution of the residual stress direction-field. In addition, the stress magnitudes are specified at a sparse set of control points, enabling the expert to adapt the stress distribution to the patient's tissue consistency. Direction and magnitude parameters are propagated to the whole body via constraint interpolation.
- *A novel stress tensor visualization method to assist the modeling process.* The visualization method is in spirit similar to how the anisotropic behavior of skin stress is observed. By making many small round incisions on the soft tissues, and simulating the deformation after these topological changes, it is easy to perceive the principle direction of residual stress and to predicate the effect of surgical operations.
- *A demonstration of the potential of the proposed method in cutting simulations.* In a number of preliminary tests we show that the residual stress distributions generated by the semi-automatic modeling process yield very realistic wound openings in virtual cutting simulations. The possibility to interactively adjust the distributions taking into account the observed tissue consistency (e.g., tight or loose) enables cutting simulations that mimic the real-world tissue behavior quite realistically.

The remainder of this paper is organized as follows: In Section 2, we review related work in biomedical engineering and visualization. In Section 3, we discuss the properties of residual stress from both a mechanical and a biological perspective, and we lay open the foundation on which our approach is based. In Section 4 and Section 5, we introduce the modeling procedure and the visualization approach, respectively. Implementation details are given in Section 6. We conclude the paper with some results and ideas for further research in this field.

2. Related Work

The accurate measurement of residual stress is still an open problem, due to the fact that the mechanical effect of the residual stress is highly coupled with the nonlinear, heterogeneous, anisotropic behavior of biological tissues. Nevertheless, both *in vivo* and *ex vivo* experiments have been performed to investigate the residual stress in soft tissues such as the skin [JJKG08, FTM11]. These experiments typically capture only the residual stress of a small specimen. However, a consistent residual stress field defined on the whole soft tissue is needed for the purpose of medical simulation. In this paper, we try to obtain a meaningful stress field by a constructive method based on the parameters modeled by domain experts.

Tensor field modeling. Zhang et al. [ZHT07] presented a topology based approach to design tensor fields on surfaces. An extension of this approach to 3D tensor fields is not trivial, since the topology of 3D tensor fields is much more complicated. Recently, Huang et al. [HTWB11] proposed a method to construct smooth 3D cross-frame fields based on a spherical harmonics representation of frames. The three axes of a cross-frame has no order, and thus the decomposition of a cross-frame field into three consistent eigenvector fields is not straightforward. Arsigny et al. [ACPA06] proposed

Log-Euclidean metrics for calculus on diffusion tensors. Our stress tensors differ from the diffusion tensors in that the stress tensor is not positive-definite. Meanwhile, the expensive evaluation of logarithms also makes this sophisticated approach not suitable for interactive modeling. Takayama et al. [TIHN07] proposed a sketch based interface to model myocardial fiber orientation, and extended it to model tensor fields for solid texturing [TOII08]. Also for solid texture synthesis, Zhang et al. [ZDL^{*}11] proposed to use quaternions to represent tensors. Our problem differs from this as the tensor field of residual stress should satisfy some equilibrium equations.

Tensor field visualization. Various tensor field visualization approaches for different applications have been proposed based on glyphs, line/surface tracing, line integral convolution, direct volume rendering, topological features [HLL97], physical effects of the tensor field on the underlying media [ZP02], or a combination of multiple of above techniques [WLY04, DGBW09]. Our visualization is close to the volume deformation based approach [ZP02]. Moreover, we perform topological operations to make the deformation more meaningful for surgery planning. It can be seen as a reproduction of Langer's experiments [Lan78] from which he observed the anisotropic behavior of skins.

3. Modeling Foundations

In this section, we shortly review the theoretical foundations of our modeling method. We first specify the equilibrium equations which the residual stress tensor field must satisfy due to the underlying physical principles. We then address the characteristics of residual stresses in the medical context of soft tissue simulation.

3.1. Mechanics of residual stress

We consider a deformable body with reference configuration $\Omega \subset \mathbb{R}^3$. The 3D second-order residual stress tensor field σ must satisfy the following equilibrium equations [Hog86]:

$$-\operatorname{div} \sigma = f_{b,0} \equiv 0 \quad \text{in } \Omega, \quad (1)$$

$$\sigma n_\Gamma = f_{s,0} \equiv 0 \quad \text{on } \Gamma_N, \quad (2)$$

$$\sigma^T = \sigma \quad (3)$$

Here, n_Γ is the unit outward normal on $\Gamma = \partial\Omega$. $\Gamma_N \subset \Gamma$ denotes the free surface of the deformable body. $f_{b,0}$ and $f_{s,0}$ denote the residual body forces and surface forces, which are applied in the undeformed state. These forces are zero in our application.

Equations (1) and (2) correspond to the fact that the residual stress and the residual body and surface forces must be balanced in the undeformed state. In the absence of external forces, these equations mean that the residual stress is self-balanced at each material point, and that on the surface the residual stress perpendicular to the surface must be zero.

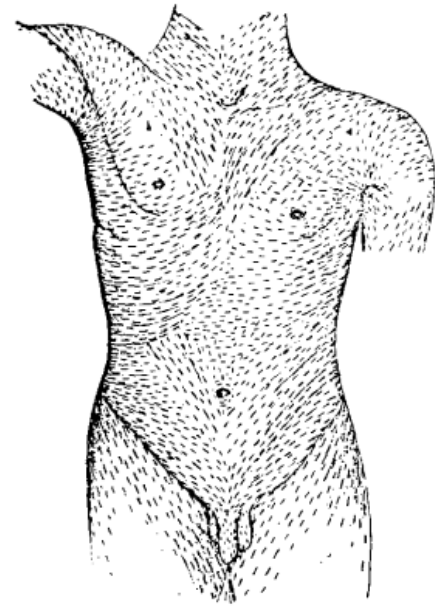


Figure 2: Directions of highest tension within the human skin (illustration by anatomist Langer [Lan61], 1861).

By integrating these equations over the body's domain and surface, it can then be derived that the mean residual stress within the body is zero [Hog86]. This implies that a non-zero uniform residual stress tensor field cannot exist.

Equation (3) specifies that the stress tensor is symmetric. According to the spectral decomposition theorem, a 3D second-order, symmetric tensor can be decomposed into three mutually orthonormal eigenvectors n_i and three eigenvalues λ_i according to

$$\sigma = \sum_{i=1}^3 \lambda_i n_i \otimes n_i, \quad (4)$$

where \otimes denotes the tensor product operator. A positive eigenvalue means that the body is tensioned along its corresponding eigenvector direction, whereas a negative eigenvalue means that the body is compressed along this direction. Note that the directions of the eigenvectors are not unique—if v is an eigenvector, then $-v$ also is an eigenvector. Therefore, when we refer to the direction of an eigenvector v , we rather refer to the (non-oriented) direction of the line $\lambda v, \lambda \in \mathbb{R}$.

3.2. Residual stress in soft tissues

The decomposition of the stress tensor into eigenvectors and eigenvalues is meaningful in anatomy and physiology. A well-known concept in plastic and reconstructive surgery are *cleavage lines*, which were first described in 1861 by anatomist Karl Langer [Lan61], and thus are also named as *Langer's lines*. Langer's work was initially written in German language, and later translated into English by Gibson

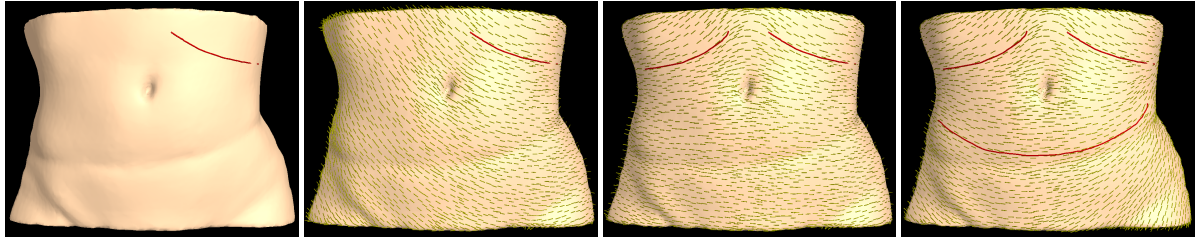


Figure 3: Modeling the eigenvector field by sketching on the surface. The vector field (yellow arrows) is created after the user draws the first stroke (red line), and updated every time after the user draws a new stroke.

[Lan78]. One of the original illustrations by Langer is shown in Figure 2. It depicts directions within the human skin along which the skin has the highest tension—mathematically, this direction at each point is the direction of the eigenvector corresponding to the largest eigenvalue. A surgical cut is usually carried out parallel to Langer’s lines, since parallel incisions generally heal better and produce less scarring than those which cut across.

Biologically, Langer’s lines correspond to the natural orientation of collagen fibers within the dermis. In general, the residual stresses in soft tissues are highly related to the growth of organs [GO06]. According to the model of kinematic growth [KHM94], residual stresses are developed during the growth of soft tissue in the following way: The original body is fictitiously decomposed into many small stress-free pieces, each of which grows independently. Because the growths in each piece need not be compatible, internal forces are needed to assemble the pieces into a consistent configuration. These internal forces induce residual stresses. Since the growth of soft tissues is slow and gradual, it can be assumed that the residual stresses vary smoothly throughout the tissue.

4. Modeling Procedure

Based on the spectral decomposition of the stress tensor, we construct the stress tensor field by modeling eigenvector and eigenvalue fields. Assuming that the residual stress field in biological tissues is smooth, we propose the following approach: The user specifies eigenvectors and eigenvalues at a few, sparsely distributed locations on the surface of the object. These values are smoothly propagated over the entire domain of the body by using Laplacian interpolation, with the equilibrium equations serving as a regularization term. After the residual stress tensor field has been computed, the effect of this field on the underlying media (augmented by a set of cuts) is immediately visualized (see Section 5). Following a computational steering approach, the domain expert can then further refine the eigenvector and eigenvalue fields, until the desired result is obtained (see Figure 1 for an illustration of this process).

In the modeling process, we first specify the eigenvector fields, followed by the eigenvalue fields. Since the three

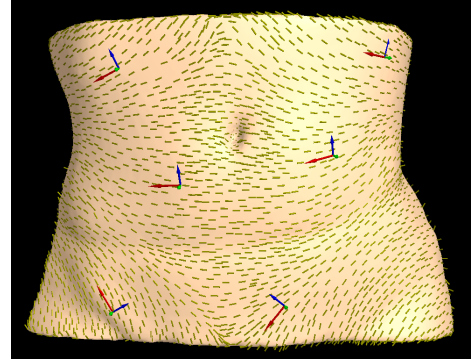


Figure 4: Modeling the eigenvalue fields by adjusting frame-arrow lengths. The local tensor frame (colored arrows) of a user-selected location shows the specified eigenvalue along each direction.

eigenvectors at each point are mutually orthogonal, it is sufficient to specify two eigenvectors—the third eigenvector can be obtained by computing their cross product. Moreover, the normal on the surface is an eigenvector of the stress tensor (since $\sigma n = 0$ on Γ_N , i.e., n is eigenvector for the eigenvalue 0). Therefore, only one eigenvector field must be specified by the user, corresponding to Langer’s lines.

To specify this field for a patient specific geometry model, the user draws a set of strokes on the surface of the body. From these strokes, a smooth vector field in the entire body is constructed and visualized. As the user incrementally draws more strokes, the vector field is further refined. An example of user input strokes and the automatically constructed eigenvector field is shown in Figure 3.

The eigenvalue fields are specified in a similar way. Since the eigenvalue corresponding to the surface normal is always zero, up to two eigenvalues can be specified at a point. Considering the user interface, after the user has selected a location on the surface, we show the local tensor frame with colored arrows indicating the direction of surface normal, the Langer’s line, and the third vector resulting from their cross product. The length of the arrow corresponds to the magnitude of the eigenvalue as it is specified by the user (see Figure 4).

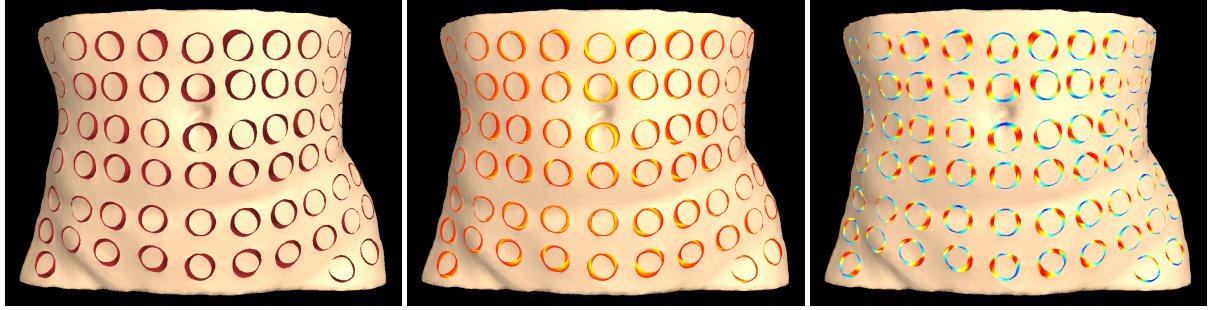


Figure 5: Left: A visualization of the residual stress tensor by simulating the effect of many small round incisions. The long axis of the outer ellipse corresponds to the major principle direction, while the width of the wound gives a direct visual impression how the tissue behaves when being cut. Middle: The resulting cutting surfaces are colored by the depth. Right: The cutting surfaces are colored by the magnitude of the residual stress component in the direction of the cutting surface normal.

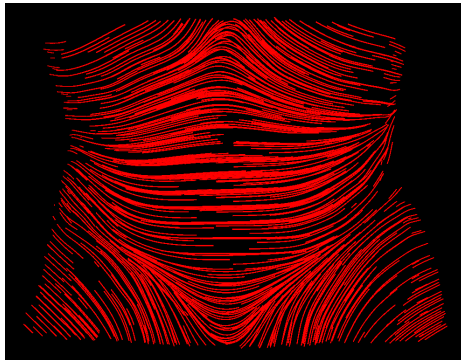


Figure 6: A streamline visualization of the interpolated 3D volumetric eigenvector field.

5. Visualization

The residual stress tensor field could be visualized by showing streamlines that are traced in the eigenvector fields (see Figure 6). However, from such a visualization it is rather difficult for the surgeon to interpret the physical behavior of the material after cutting, which depends on not only the residual stresses, but also the material properties, and the depth and the length of an incision. Therefore, for our particular application, we propose a visualization method which directly shows this behavior.

Our method is based on introducing a set of small, round incisions distributed over the surface of the body. Then, the deformation of the body due to the residual stress is computed (see Figure 5). Typically, due to the relaxation of residual stress after cutting, the body will shrink, and the wounds will open. If the residual stress is anisotropic, both the outer and inner wound margins become elliptical in shape with their axes mutually orthogonal (see Figure 7). The major axis of the outer ellipse indicates the eigenvector direction for the major eigenvalue. On the surface, it corresponds to Langer's lines. The gap between the outer and inner boundary of the wound indicates the magnitude of the stress.

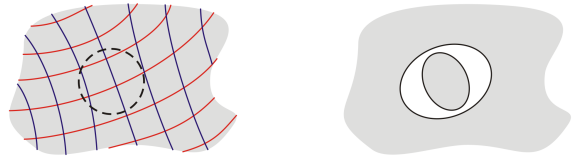


Figure 7: Left: An eigenvector field (red and blue curves) of the residual stress, the eigenvalues along the red curves are larger than those along the blue ones. Right: After a round incision (the dashed circle), the wound gapes.

This visualization approach is similar to how Langer observed the anisotropic phenomenon of the residual stress [Lan78]. Langer marked circular outlines at short distances from each other on the skin of cadavers, and then incised around the circles. From the resulting deformation he observed patterns and determined "line directions" by the longer axes of the outer wound margins.

We provide two coloring approaches of the new cutting surface to better indicate some important information, i.e., the depth of the cutting, and the stress in the direction normal to the cutting surface. The depth field is computed in a way similar to Takayama et al. [TOII08]. We define the skin layer of the abdomen wall as having depth 0 (red color), and the inner layer as having depth 1 (yellow color). Radial based function interpolation is then used to interpolate the depth values.

To better visualize the anisotropic behavior of the deformation, we color the cutting surface by the norm of the normal component of the residual stress, $\|\sigma n\|_2$, where n represents the normal of the newly created cutting surface, with a linear color map from red for the highest tension to blue for the lowest. These colors are consistent with the color of arrows for eigenvalue editing. As we can see from Figure 5 right, the red area means higher released tension, while blue area means lower tension. The axis passing through red poles indicates the Langer's line.

6. Implementation

In this section, we introduce the interpolation of residual stress tensors (i.e., eigenvector fields and eigenvalues fields), and the dynamic simulation of deformable bodies with residual stresses. The eigenvector fields are interpolated by Laplacian smoothing, while the eigenvalue fields are interpolated by combining the Laplacian equation and the static equilibrium equation in a least square sense. It is arguable that an interpolation approach which treats the whole tensor as a unity may produce more reasonable results. However, since the tensor is preferably represented by eigenvectors and eigenvalues for intuitive modeling inputs, and they are of different units and scales, the resulting formulation of optimization problem in that case is ill conditioned and its convergence is poor. Thus, we choose to generate the tensor field by interpolating eigenvectors first and then eigenvalues.

Our interpolation and simulation are based on a hexahedral finite element discretization using a uniform Cartesian grid, following the approach proposed in [DGW11] and [WDW11]. The topology of the finite element model is represented by using a linked volume, where face-adjacent elements are connected via links, and these links are marked as disconnected when the respective elements are separated by a cut. A visually smooth render surface that is topologically consistent with the hexahedral finite element model is constructed directly from this model by using a dual-contouring approach. For details, we refer the reader to the original works.

For the modeling of the residual stress tensor field, the user paints eigenvectors and eigenvalues onto the smooth render surface. The respective values are propagated to the closest hexahedral finite elements. The computation of the residual stress tensor field is then performed on this grid.

6.1. Static equilibrium equations

For the discretization of the continuous equilibrium equations, we employ a hexahedral finite element discretization using piecewise constant interpolation for the residual stress tensor field (i.e., we store one stress tensor per element) and trilinear interpolation for the test functions. This leads to a linear system of equations

$$T\bar{\sigma} = 0. \quad (5)$$

Here, $\bar{\sigma}$ is a linearization of the per-element stress tensors, each of which is represented as a 6-component vector $\bar{\sigma}^e = (\sigma_{11}^e, \sigma_{22}^e, \sigma_{33}^e, \sigma_{12}^e, \sigma_{13}^e, \sigma_{23}^e)^T$ using Voigt notation. T is an $n_v \times n_e$ matrix which maps per-element stress tensors to per-vertex forces, where n_e and n_v denote the number of finite elements and vertices, and each matrix entry is itself a matrix consisting of 3×6 scalars. T is assembled from the per-element matrices

$$T^e = \int_{\Omega^e} (B^e)^T dx,$$

by considering the sharing of vertices between adjacent finite elements. Here, $B^e(x)$ is the element strain matrix, and Ω^e is the domain of the finite element. Note that the matrix T depends only on the geometry and topology of the deformable body; it does *not* depend on the material properties such as Young's modulus or Poisson's ratio.

For eigenvalue interpolation, we employ a formulation of Equation (5) in terms of eigenvalues. According to Equation (4), it is given by

$$T \frac{d\bar{\sigma}}{d\lambda} \lambda = 0, \quad (6)$$

where λ is a linearization of the per-element stress tensors' eigenvalues, and $\frac{d\bar{\sigma}}{d\lambda}$ is assembled from the per-element third-order tensors $\frac{d\sigma^e}{d\lambda^e}$ given by

$$\left(\frac{d\sigma^e}{d\lambda^e} \right)_{ijk} = (n_k^e \otimes n_k^e)_{ijk}.$$

6.2. Interpolation of eigenvalues

In the following, we introduce our interpolation scheme for the case of eigenvalue interpolation. The interpolation of the eigenvectors, which is algorithmically performed *prior* the interpolation of the eigenvalues, is performed in a similar way and is described in the following section.

For the formulation of our interpolation scheme, we consider a vector-valued function $\phi(i) = \lambda^i = (\lambda_1^i, \lambda_2^i, \lambda_3^i)^T$, which specifies the three eigenvalues for each finite element $i = 1, \dots, n_e$.

Laplacian operator: We use Laplacian smoothing [SCOL*04] to propagate the prescribed values over the entire domain of the body. The discrete Laplacian operator Δ acting on ϕ is defined as

$$(\Delta\phi)(i) = \sum_{j \in N_1(i)} \omega(i, j) [\phi(j) - \phi(i)],$$

where $N_1(i)$ is the set of elements that are face-adjacent to element i . Since we use a uniform discretization, the weight $\omega(i, j)$ is chosen as $\omega(i, j) = \frac{1}{|N_1(i)|}$. To get a smooth tensor field, we seek for

$$(\Delta\phi)(i) = 0, \quad i = 1, \dots, n_e.$$

In matrix form, this is written as

$$L\lambda = 0, \quad (7)$$

where $\lambda = ((\lambda^1)^T, \dots, (\lambda^n)^T)^T$, and L is an $n_e \times n_e$ matrix defined by

$$L_{ij} = \begin{cases} -I_{3 \times 3} & \text{if } i = j, \\ \omega(i, j) I_{3 \times 3} & \text{if } j \in N_1(i), \\ 0 & \text{otherwise.} \end{cases}$$

Boundary condition: The eigenvalues for some elements

are prescribed by the user. This is modeled by

$$\phi(i_k) = \lambda^{i_k,0}, \quad k = 1, \dots, n_p,$$

meaning that for element i_k the eigenvalues $\lambda^{i_k,0}$ are prescribed. n_p denotes the number of these elements. The matrix form of these constraints is given by

$$C\lambda = \lambda^0, \quad (8)$$

where $\lambda^0 = ((\lambda^{1,0})^T, \dots, (\lambda^{n_p,0})^T)^T$, and C is an $n_p \times n_e$ matrix defined by

$$C_{k\ell} = \begin{cases} I_{3 \times 3} & \text{if } \ell = i_k, \\ 0 & \text{otherwise.} \end{cases}$$

We solve the linear systems given by the Laplacian operator Equation (7), the boundary constraint Equation (8), and the equilibrium constraint Equation (6) in a least squares sense, i.e.,

$$\arg \min_{\lambda} \|A\lambda - b\|_2^2, \quad (9)$$

where $A = (L \ C \ T \frac{d\bar{\sigma}}{d\lambda})^T$, and $b = (0 \ \lambda^0 \ 0)^T$. The corresponds the linear system, $A^T A \lambda = A^T b$, is evaluated by a conjugate gradient solver.

6.3. Interpolation of eigenvectors

For the eigenvector interpolation, which is performed component-wise, the formulation of the Laplacian operator and user-specified constraints is analogous, with the exception that the equilibrium equation is not considered in the minimization problem.

Note that due to the component-wise interpolation of the eigenvectors, it is finally required to orthonormalize the resulting fields in order to obtain a set of mutually perpendicular eigenvector fields. In the orthonormalization process, the eigenvector along the normal direction is fixed, while the one along Langer's line is clipped and normalized.

6.4. Dynamic simulation

The incorporation of the residual stresses into the simulation of the deformable body leads to the spatially discretized Lagrangian equation of motion

$$T\bar{\sigma} + M\ddot{u} + D\dot{u} + Ku = f. \quad (10)$$

Here M , D , and K are the mass, damping, and stiffness matrix, and u and f are the linearized vertex displacements and per-vertex forces. Note that the matrices in this equation have to be reassembled whenever the topology of the object has changed, i.e., whenever the object has been cut. To enable the accurate simulation of large deformations using linear elasticity, we employ the corotational formulation of the linear strain tensor. The linear system of equations resulting from applying the implicit Newmark time integration scheme is solved by using an efficient geometric multigrid solver [DGW11].

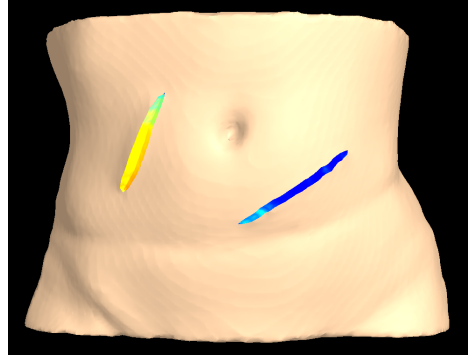


Figure 8: The left cut crosses the Langer's lines, while the right cut follows Langer's lines (the lines are shown in Figure 2). The wound caused by the cross cut is wider.

7. Results and Discussion

For our experiments, the Young's modulus and Poisson's ratio are chosen as 80 kPa and 0.4 respectively, which are comparable to those of an abdominal wall [SAF*06]. The tension along the Langer's lines is typically prescribed as 20 kPa, while along the cross direction it is 10 kPa [JJKG08]. Our experiments were run on a standard desktop PC equipped with an Intel Core Q9450 processor running at 2.66 GHz (a single core is used), 4 GB of RAM, and an NVIDIA GeForce GTX 280 graphics card.

Figure 8 shows two cuts, the left cut crosses Langer's lines, while the right one follows Langer's lines. It can be seen that the wound caused by the cross cut is wider. Figure 9 left shows the simulation of a flap surgery using the residual stress distribution computed from a reasonable modeling. Dynamic simulation is shown in the attached video. The width of the wound is typically 5 ~ 20 mm. So far, the doctors were not able to clearly differentiate the Langer's lines for different types of bodies. The doctors, however, found our simulated cuts to be in line with what they were expecting for the particular body type presented in this paper. Therefore we are planning to compare the results of our simulations to measurement of real cuts in the future.

Flap surgery simulations with residual stresses computed from different eigenvector and eigenvalue specifications are shown in Figure 9. This demonstrates the variations of wound openings depending on the residual stress distribution.

Figure 10 shows our modeling and visualization techniques applied to a cylinder model. In the upper part of the cylinder, we assign the same eigenvalue on the Langer's direction and the cross-Langer's direction. In the lower part, the eigenvalue on the cross-Langer's direction is reduced by half. As a consequence, in the upper part the shape of incisions is still circular, while those in the lower part become ellipses.

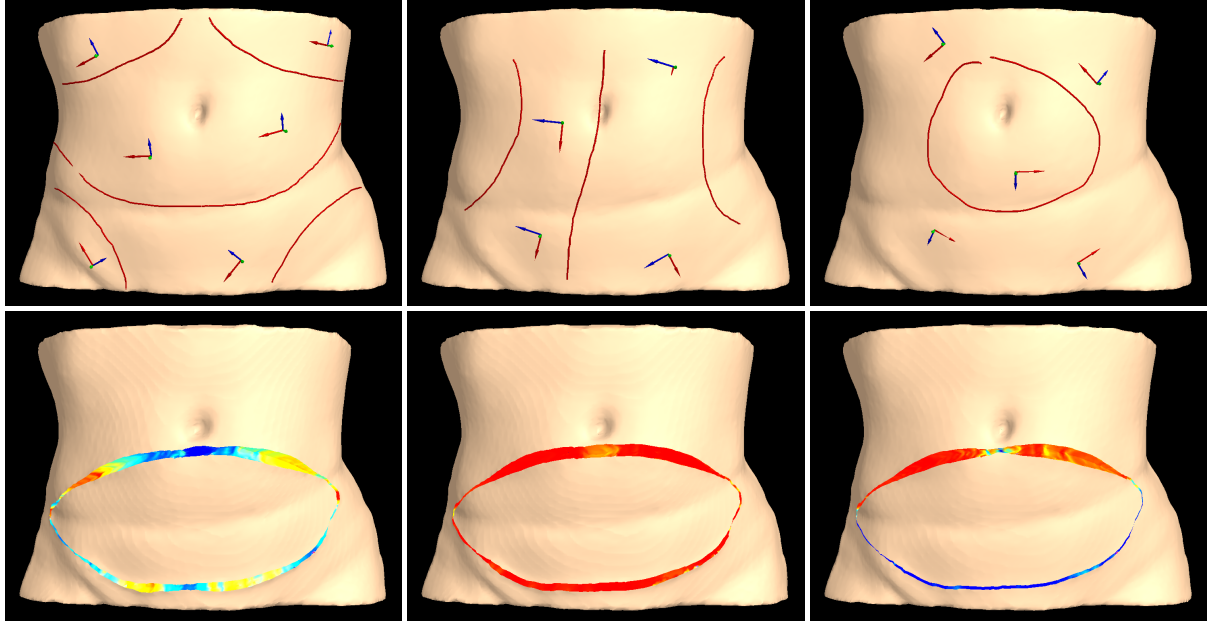


Figure 9: Top: Three different specifications of eigenvectors and eigenvalues. Bottom: Flap surgery simulations with residual stresses computed from different specifications. The cutting surfaces are colored by the magnitude of the residual stress component in the direction of the cutting surface normal.

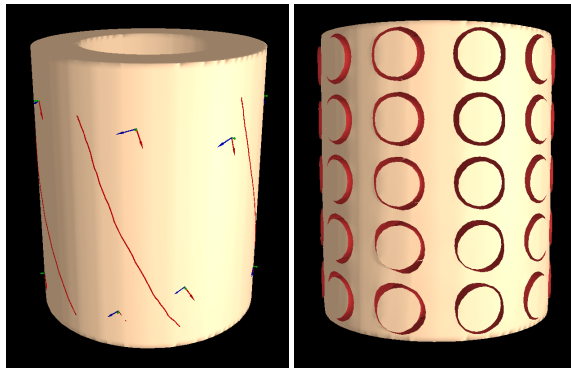


Figure 10: Modeling and visualization on a cylinder model. The stresses in the upper part are set isotropic, while that in the lower part are set anisotropic. The resulting shapes of round incisions are circular and elliptical respectively.

Table 1 shows the performance of our system for different models and different resolutions. The second group of columns gives information about the models, i.e., the resolution, the number of hexahedral finite elements, and the number of simulation vertices. The third group shows the timing statistics for each modeling step. The first column gives the time for the eigenvector interpolation, which includes the interpolation of the user-specified Langer's lines and the surface normals, orthonormalization and the computation of the third eigenvector. The next column shows time for the interpolation of the user-specified eigenvalues. The last column

gives the time for a single step of the dynamic deformation simulation. The statistics demonstrate that for models of a few thousands of cells, the model can be computed in one second. For models consisting of a few tenthousand of cells, the computations take a few seconds.

Model	Resolution	# Cells	# Vertices	Time [ms]		
				Vector	Value	Sim.
Cylinder	21×21×26	5,550	7,540	261.4	215.2	83.3
Cylinder	42×42×51	44,000	51,714	5,517	8,951	637.4
Abdomen	63×21×42	5,734	10,189	155.6	106.1	98.6
Abdomen	126×41×84	45,313	62,481	3,046	3,607	707.8

Table 1: Performance statistics for different models and different resolutions. The last three columns give times for the eigenvector interpolation, the eigenvalue interpolation, and the dynamic simulation, respectively.

8. Conclusion and Future Work

We have presented methods to design and visualize a patient-specific residual stress tensor field with respect to physical constraints. The design is based on the mechanics of residual stress in soft biological tissues. We proposed a method for interactively designing tensor fields via a sketch-based interface. A graphical depiction of the residual stress distribution is achieved by visualizing the simulated deformations of a set of small round incisions. In a number of examples we demonstrated the potential of our approach in patient-specific surgery simulation, where a consistent residual stress tensor is desired.

Our method is well suited for modeling the residual stress distribution on shell-like structures, which are common in biological tissues. For complex-shaped structures, it would be interesting to allow the user to draw stress directions inside the body, if the user has *prior* knowledge of the interior residual stress. Meanwhile, as a modeling tool, the accuracy of its results depends heavily on the correctness of user's inputs. Thus it would be beneficial to incorporate into the modeling framework accurate measurements of some parameters as a complement to surgeon's experience. Another issue is that the user-sketched stroke has a specific direction, while the eigenvector of a tensor is actually bidirectional. This specification may produce some artifacts in vector field generation. Further investigation is needed to address this open problem.

In the future we will also investigate the parallelization of our approach on GPU and Multicore-CPU architectures. Even though our method already achieves quite satisfying update rates, it can still take several seconds to update a residual stress field with respect to the user input. In order to achieve good scalability on a parallel system, we will in particular address the integration of iterative solution methods into our approach. Furthermore, we will evaluate the confidence of our results with respect to real-world measurement. It is planned for the near future to measure and compare with the shrinkage of flaps in breast reconstruction surgery using the same patient model.

9. Acknowledgments

We thank Dr. med. Laszlo Kovacs at TU München for providing the abdomen wall model, and anonymous reviewers for insightful comments to improve the manuscript. The first author, Jun Wu, is supported by the Erasmus Mundus TANDEM, an European Commission funded program. This publication is based on the SINUS III project funded by the German Federal Ministry of Economics and Technology.

References

- [ACPA06] ARSIGNY V., COMMOWICK O., PENNEC X., AYACHE N.: A log-euclidean framework for statistics on diffeomorphisms. In *Proc. MICCAI* (2006), pp. 924–931. [2](#)
- [CF86] CHUONG C.-J., FUNG Y.-C.: On residual stresses in arteries. *J. Biomech. Eng.* 108, 2 (1986), 189–192. [1](#)
- [DGBW09] DICK C., GEORGII J., BURGKART R., WESTERMANN R.: Stress tensor field visualization for implant planning in orthopedics. *IEEE Trans. Vis. & Comput. Graph. (Proc. IEEE Visualization)* 15, 6 (2009), 1399–1406. [3](#)
- [DGW11] DICK C., GEORGII J., WESTERMANN R.: A hexahedral multigrid approach for simulating cuts in deformable objects. *IEEE Trans. Vis. & Comput. Graph.* 17, 11 (2011), 1663–1675. [6, 7](#)
- [FTN11] FLYNN C., TABERNER A., NIELSEN P.: Mechanical characterisation of in vivo human skin using a 3d force-sensitive micro-robot and finite element analysis. *Biomechanics and Modeling in Mechanobiology* 10 (2011), 27–38. [2](#)
- [GO06] GUILLOU A., OGDEN R.: Growth in soft biological tissue and residual stress development. In *Mechanics of Biological Tissue*, Holzapfel G. A., Ogden R. W., (Eds.). 2006, pp. 47–62. [4](#)
- [HLL97] HESSELINK L., LEVY Y., LAVIN Y.: The topology of symmetric, second-order 3D tensor fields. *IEEE Trans. Vis. & Comput. Graph.* 3, 1 (1997), 1–11. [3](#)
- [Hog86] HOGER A.: On the determination of residual stress in an elastic body. *Journal of Elasticity* 16 (1986), 303–324. [3](#)
- [HTWB11] HUANG J., TONG Y., WEI H., BAO H.: Boundary aligned smooth 3d cross-frame field. *ACM Trans. Graph.* 30, 6 (2011), 143:1–143:8. [2](#)
- [Hum03] HUMPHREY J.: Review paper: Continuum biomechanics of soft biological tissues. *Proc. Royal Society of London. Series A 459*, 2029 (2003), 3–46. [1](#)
- [JJKG08] JACQUET E., JOSSE G., KHATYR F., GARCIN C.: A new experimental method for measuring skin's natural tension. *Skin Research and Technology* 14, 1 (2008), 1–7. [2, 7](#)
- [KHM94] K.RODRIGUEZ E., HOGER A., MCCULLOCH A. D.: Stress-dependent finite growth in soft elastic tissues. *J. Biomech.* 27, 4 (1994), 455–467. [4](#)
- [KZPB04] KOVACS L., ZIMMERMANN A., PAPADOPULOS N. A., BIEMER E.: Re: factors determining shape and symmetry in immediate breast reconstruction. *Annals of Plastic Surgery* 53, 2 (2004), 192–194. [1](#)
- [Lan61] LANGER K.: Zur anatomie und physiologie der haut. über die spaltbarkeit der cutis. *Sitzungsbericht der Mathematisch-naturwissenschaftlichen Classe der Wiener Kaiserlichen Academie der Wissenschaften Abt* (1861), 44. [3](#)
- [Lan78] LANGER K.: On the anatomy and physiology of the skin. *British journal of plastic surgery* 31 (1978), 3–8, 93–106. Translated by T. Gibson. [2, 3, 4, 5](#)
- [SAF*06] SONG C., ALIJANI A., FRANK T., HANNA G., CUSCHIERI A.: Elasticity of the living abdominal wall in laparoscopic surgery. *J. Biomech.* 39, 3 (2006), 587 – 591. [7](#)
- [SCOL*04] SORKINE O., COHEN-OR D., LIPMAN Y., ALEXA M., RÖSSL C., SEIDEL H.-P.: Laplacian surface editing. In *Proc. Symp. on Geometry Processing* (2004), pp. 175–184. [6](#)
- [TIHN07] TAKAYAMA K., IGARASHI T., HARAGUCHI R., NAKAZAWA K.: A sketch-based interface for modeling myocardial fiber orientation. In *Proc. the 8th international symposium on Smart Graphics* (2007), pp. 1–9. [3](#)
- [TOII08] TAKAYAMA K., OKABE M., IJIRI T., IGARASHI T.: Lapped solid textures: Filling a model with anisotropic textures. *ACM Trans. Graph.* 27, 3 (2008), 53:1–53:9. [3, 5](#)
- [WDW11] WU J., DICK C., WESTERMANN R.: Interactive high-resolution boundary surfaces for deformable bodies with changing topology. In *Proc. Workshop on Virtual Reality Interaction and Physical Simulation (VRIPHYS)* (2011), pp. 29–38. [6](#)
- [WLY04] WÜNSCHE B. C., LOBB R., YOUNG A. A.: The visualization of myocardial strain for the improved analysis of cardiac mechanics. In *Proc. Computer graphics and interactive techniques in Australasia and South East Asia* (2004), pp. 90–99. [3](#)
- [ZDL*11] ZHANG G.-X., DU S.-P., LAI Y.-K., NI T., HU S.-M.: Sketch guided solid texturing. *Graphical Models* 73, 3 (2011), 59 – 73. [3](#)
- [ZHT07] ZHANG E., HAYS J., TURK G.: Interactive tensor field design and visualization on surfaces. *IEEE Trans. Vis. & Comput. Graph.* 13, 1 (2007), 94–107. [2](#)
- [ZP02] ZHENG X., PANG A.: Volume deformation for tensor visualization. In *Proc. IEEE Visualization* (2002), pp. 379–386. [3](#)